R. G. Nazmitdinov; Jan Kvasil
Shape evolution of rotating nuclei

Acta Universitatis Carolinae. Mathematica et Physica, Vol. 33 (1992), No. 1, 3--36

Persistent URL: http://dml.cz/dmlcz/142642

Shape Evolution of Rotating Nuclei

R. G. NAZMITDINOV*) AND JAN KVASIL**)

USSR, Czechoslovakia

Received 30 August 1990

The paper is devoted to the studying of the effects connected with the deexcitation of nuclear states with high spins and high excitation energy. It is shown that process of deexcitation is influenced mainly by the deformation of nucleus in given angular momentum and excitation energy (nuclear temperature). The way of deexcitation (particle emmision or emmision of γ-quanta energy (nuclear temperature). The way of deexcitation (particle emmision or emmision of γ-quanta), the spectrum of emmited particles and half times of excited states depends on the nuclear shape. This dependence is demonstrated in this paper for a number of nuclei.

V práci jsou studovány efekty spojené s deexcitací stavů s vysokým spinem a s vysokou excitační energií v atomových jádrech. Pozornost je věnována zejména jevům souvisejícím s evolucí tvaru jádra s rostoucí úhlovou frekvencí rotace jádra. Je ukázáno, že proces deexcitace vysoceexcitovaných stavů s velkým spinem je do značné míry ovlivněn deformací jádra při daném spinu a excitační energii (jaderné teplotě). Způsob deexcitace (částicová emise nebo emise γ-kvant), tvary spekter emitovaných částic resp. poločasy rozpadu excitovaných stavů závisí na tvaru resp. deformaci jádra. Tato závislost je v práci demonstrována na řadě jader.

В работе анализируются эффекты связанные с девозбуждением ядерных состояний с большим спином и с большой энергией возбуждения ядер. Работа посвящена главным образом явлениям вызванным изменением формы ядер при их вращении. В работе показано, что деформация ядра решающим образом влияет на процесс девозбуждения состояний с большим спином и большой температуой. Способ девозбужения (испускание частиц или испускание γ-квантов), форма спектер испускаемых частиц и время жизни возбужденных состояний зависит от формы или деформации ядра. Эта зависимость в работе демонстрируется на ряду ядер.

1. Introduction

High spin states of atomic nuclei are usually obtained in (HI, xn) or (α, xn) reactions [1, 2]. As a result of these reactions the compound-nucleus is formed in the states with high angular momenta and high excitation energies. In the first step of the following deexcitation the neutrons and light charged particles are evaporated.

*) Laboratory of Theoretical Physics, JINR Dubna, SV 101 00, USSR.

**) Department of Nuclear Physics, Faculty of Mathematics and Physics, Charles University, V Holešovičkách 2, 180 00 Praha 8, Czechoslovakia.

In this process considerable part of excitation energy and very small part of angular momentum are taken away. Then the deexcitation of high-spin states of rotating nucleus is realised by means of dipole and quadrupole gamma quanta. In these transitions the nucleus comes from the region of high density of states to the region near the yrast line where the state density is not so high however nucleus angular momentum keeps its high value. Then the deexcitation of nucleus continues by the electromagnetic translations along the yrast line and loosing its angular momentum the nucleus reaches the ground rotational band at the values of angular momentum $I \sim (18-20)\,\hbar$.

Products of heavy ion reactions are characterised by high excitation energy which are spred over a lot of different nuclear degrees of freedom [3]. Therefore the analysis of such experiments depends on the knowledge of all factors determining the evolution of products of (HI, xn) reactions. One of the most important factors in this sense is the nuclear shape (deformation parameters) as well as deformation energy and inertical nuclear properties. In calculation of equilibrium shape of rotating nucleus one can distinquish two limiting cases of approach. The first one is based on liquid drop model which corresponds to the case of nucleus excited to the extend when the shell effects do not play any role. The opposite case is represented by papers where the shell effects are involved in terms of Strutinsky-shell corrections. This paper is mainly devoted to the intermediate case with nuclear excitation energy lying betweeen two limits mentioned above.

The analysis of high excited nuclear states is usually performed in terms of statistical approaches. Statistical characteristics of excited nuclei are similar to high extend to that of ideal Fermi-gas. However the Fermi gas model does not involve some nuclear specifics such as shell effects. In this paper it is shown how the shell effects can be included in calculation of the equilibrium characteristics of cold as well as heated rotating nuclei in the framework of cranking model.

The investigation of the equilibrium shape of fast rotating nuclei is usually carried out under the following assumptions.

i) The cranking model is applicable for a broad interval of rotation frequences starting from the low-spin region up to the highest frequences in which the nucleus can exist as a bound system.

ii) In practical calculations the nuclear average field is approximated by deformed Nilsson or Wood-Saxon potential. The parameters of this potential are supposed to be independent on nuclear angular momentum with the exception of deformation parameters of nuclear shape.

iii) Dominant part of binding energy varies smoothly from one nucleus to another and it can be determined in the framework of liquid drop model, the surface parameter of which is independent on angular momentum. This assumption is justified for heavier nuclei with $A > 40$.

All the assumptions mentioned above were used in this paper and the comparison of our results with heavy ion reaction data approved them. It has to be mentioned

that these assumptions are applicable not only for yrast-line states but also for excited states.

This paper represents the review of our results concerning the selfconsistent study of the shape evolution of cold as well as heated rotating nuclei. It also involves the disscussions of possible physical effects caused by the shape changes of nucleus which are directly connected with data observed or observable in experiments.

2. Description of yrast line

In this part of paper the yrast line states (cold nucleus) are investigated in the framework of Cranked-Hartree-Fock-Bogoliubov model. The analysis of yrast line represents the first step of investigation of the collective as well as noncollective degrees of freedom in fast rotating nuclei by means of Cranked-Hartree-Fock-Bogoliubov + Random Phase approximation (CHFB+RPA model).

We start with the HFB equations of motion for cranking model (see eq. (12) in [6]) for unknown amplitudes A_α^i, $B_{\bar\alpha}^i$ or $A_\alpha^{\bar\imath}$, $B_{\bar\alpha}^{\bar\imath}$ of canonical Bogoliubov-Valatin transformation. These equations provide also quasiparticle spectrum E_i, $E_{\bar\imath}$ in dependence on angular velocity Ω of rotation of nucleus. Since we assume the $R_x(\pi)$-symmetry of rotating nucleus there is the connection between $(A_\alpha^i, B_{\bar\alpha}^i, E_i)$ and $(A_k^{\bar\imath}, B_k^{\bar\imath}, E_{\bar\imath})$ (see [6, 7])*)

$$A_\alpha^i = B_\alpha^{\bar\imath}\,, \quad A_{\bar\alpha}^{\bar\imath} = B_{\bar\alpha}^i\,, \quad E_i = -E_{\bar\imath} \tag{1}$$

Therefore it is sufficient to solve only one system of equations from thats given in eq. (12) in [6] in order to obtain the complete ensemble of solutions of HFB problem. The procedure of solving this system of equations is usually carried out with the approximation of Nilsson or Saxon-Woods average field. This means the single-particle spherical field energy terms and the terms containing the expectation values $\langle\Omega|\, Q_{20}|\Omega\rangle\ \langle\Omega|\, Q_2^{(+)}|\Omega\rangle$ of quadrupole operators in quasiparticle vacuum $|\Omega\rangle$ given rotational frequency Ω in eq. (12) of [6] are substituted by corresponding matrix element of Nilsson average field, i.e.

$$e_\alpha\delta_{\alpha\beta} - \varkappa_2\langle\Omega|\, Q_{20}|\Omega\rangle\,\langle\alpha|\, Q_{20}|\beta\rangle - \varkappa_2\langle\Omega|\, Q_2^{(+)}|\Omega\rangle\,\langle\alpha|\, Q_2^{(+)}|\beta\rangle = \varepsilon_{\alpha\beta} \tag{2}$$

where $\varepsilon_{\alpha\beta}$ represent matrix elements of Nilsson field. In such a way the eq. (12) in [6] for amplitudes A_α^i, $B_{\bar\alpha}^i$ and for corresponding quasiparticle energies E_i can be rewritten as follows

$$\begin{pmatrix} \varepsilon_{\alpha\beta} - \lambda\delta_{\alpha\beta} - \Omega j^x_{\alpha\beta} & \Delta\delta_{\alpha\bar\beta} \\ \Delta\delta_{\bar\alpha\beta} & -\varepsilon_{\alpha\bar\beta} + \lambda\delta_{\bar\alpha\bar\beta} + \Omega j^x_{\bar\alpha\bar\beta} \end{pmatrix} \begin{pmatrix} A_\alpha^i \\ B_{\bar\alpha}^i \end{pmatrix} = E_i \begin{pmatrix} A_\alpha^i \\ B_{\bar\alpha}^i \end{pmatrix} \tag{3}$$

where λ and Δ are Fermi level and gap parameter. This equation has to be added by the conditions of number of particle conservation

$$N = \sum_{\substack{i\alpha \\ E_i<0}} (A_\alpha^i)^2 + \sum_{\substack{i\alpha \\ E_i>0}} (B_{\bar\alpha}^i)^2 \tag{4}$$

*) Throughout this paper the same notation is used as in 6.

Since the quantity Δ depends on unknown amplitudes A^i_α, $B^i_{\bar\alpha}$ (see [6])

$$\Delta = G \sum_{\substack{i\alpha \\ E_i>0}} (B^i_{\bar\alpha} A^i_\alpha) \tag{5}$$

the equation (3) represents the nonlinear selfconsistent equations and it must be solved by means of iterations. The way how to obtain changes $d\lambda$ and $d\Delta$ of Fermi energy gap in each iteration is described bellow.

For given value of rotational frequency Ω the number of particles N and pairing strength constant G can be understood formally as functions of Fermi energy λ and energy gap Δ (through the amplitudes A^i_α and $B^i_{\bar\alpha}$ and eq. (3)). Therefore

$$\begin{aligned} dN &= \frac{\partial N}{\partial \lambda} d\lambda + \frac{\partial N}{\partial \Delta} d\Delta \\ dG &= \frac{\partial G}{\partial \lambda} d\lambda + \frac{\partial G}{\partial \Delta} d\Delta \end{aligned} \tag{6}$$

The equations (6) can be used for determination of $d\lambda$ and $d\Delta$. In numerical calculations the differentials dN and dG were taken as ≈ 0.001. That means they had fixed values for all iterations. In order to obtain $d\lambda$ and $d\Delta$ from (6) we must determine the quantities $\partial N/\partial\lambda$, $\partial N/\partial\Delta$, $\partial G/\partial\lambda$ and $\partial G/\partial\Delta$.

Let us introduce the quantity F

$$F = \frac{\Delta}{G} = \sum_{\substack{i\alpha \\ E_i>0}} (B^i_{\bar\alpha} A^i_\alpha) . \tag{7}$$

From (7) one can see that

$$\frac{\partial G}{\partial \Delta} = \frac{1}{F} - \frac{\Delta}{F^2}\frac{\partial F}{\partial \Delta} = \frac{1}{F^2}\left(F - \Delta \frac{\partial F}{\partial \Delta}\right) \tag{8a}$$

$$\frac{\partial G}{\partial \lambda} = - \frac{\Delta}{F^2}\frac{\partial F}{\partial \lambda} \tag{8b}$$

The relation (4) yields

$$\begin{aligned} \frac{\partial N}{\partial \lambda} &= 2\left\{ \sum_{\substack{i\alpha \\ E_i<0}} A^i_\alpha \frac{\partial A^i_\alpha}{\partial \lambda} + \sum_{\substack{i\alpha \\ E_i>0}} B^i_\alpha \frac{\partial B}{\partial \lambda} \right\} \\ \frac{\partial N}{\partial \lambda} &= 2\left\{ \sum_{\substack{i\alpha \\ E_i>0}} A^i_\alpha \frac{\partial A^i_\alpha}{\partial \lambda} + \sum_{\substack{i\alpha \\ E_i<0}} B^i_\alpha \frac{\partial B^i_{\bar\alpha}}{\partial \lambda} \right\} \end{aligned} \tag{9}$$

So it remains to determine the quantities $\partial A^i_\alpha/\partial\lambda$, $\partial A^i_\alpha/\partial\Delta$, $\partial B^i_{\bar\alpha}/\partial\lambda$, $\partial B^i_{\bar\alpha}\partial\Delta$. They can be obtained by means of perturbation theory using standard quantum mechanics. According to definition the amplitudes $A^i_{\bar\alpha}$, B^i_α form the components of eigenvectors of HFB hamiltonian

$$H_{\mathrm{HFB}}|\nu_i\rangle = E_i|\nu_i\rangle \tag{10}$$

where $|\nu_i\rangle = |A^i_{\alpha=1} \ldots A^i_{\alpha=n}, B^i_{\bar\alpha=1} \ldots B^i_{\bar\alpha=n}\rangle$. The small change $d\lambda$ of Fermi energy λ

gives rise to perturbation term

$$\hat{V}_\lambda = -\mathrm{d}\lambda\, \delta_{\alpha\beta}\, \mathrm{sign}\,(\alpha) \tag{11}$$

so after this change the HFB hamiltonian becomes

$$H'_{\mathrm{HFB}} = H_{\mathrm{HFB}} + \hat{V}_\lambda \tag{12}$$

Using perturbation theory the perturbed wave function $|v'_i\rangle$ corresponding to unperturbed on $|v_i\rangle$ is

$$|v'_i\rangle = |v_i\rangle - \mathrm{d}\lambda \sum_{m \neq i} \frac{\langle v_m|\, \delta_{\alpha\beta}\, \mathrm{sign}\,(\alpha)|v_i\rangle}{E_i - E_m}\, |v_m\rangle = |v_i\rangle + \mathrm{d}\lambda \frac{\partial |v_i\rangle}{\partial \lambda}$$

Therefore

$$\frac{\partial |v_i\rangle}{\partial \lambda} = -\sum_{m \neq i} \frac{\langle v_m|\, \delta_{\alpha\beta}\, \mathrm{sign}\,(\alpha)\, |v_i\rangle}{E_i - E_m}\, |v_m\rangle = \sum_{\substack{\alpha \\ m \neq i}} \frac{A^m_\alpha A^i_\alpha - B^m_{\bar\alpha} B^i_{\bar\alpha}}{E_m - E_i}\, |v_m\rangle\,. \tag{14}$$

Similarly the small change $\mathrm{d}\Delta$ of energy gap Δ gives rise to perturbation

$$\hat{V}_\Delta = \mathrm{d}\Delta\, \delta_{\alpha\bar\beta} \tag{15}$$

and in analogy with (13) and (14) one obtains

$$\frac{\partial |v_i\rangle}{\partial \Delta} = \sum_{m \neq i} \frac{\langle v_m|\, \delta_{\alpha\bar\beta}|v_i\rangle}{E_i - E_m}\, |v_m\rangle = \sum_{\substack{\sigma \\ m \neq i}} \frac{A^m_\alpha B^i_{\bar\alpha} + B^m_{\bar\alpha} A^i_\alpha}{E_i - E_m}\, |v_m\rangle\,. \tag{16}$$

Substituting single components of (14) and (16) into (9) the derivatives $\partial N/\partial\lambda$ and $\partial N \partial \Delta$ can be rewritten as follows

$$\frac{\partial N}{\partial \lambda} = 2\left\{ \sum_{\substack{i\alpha \\ E_i<0}} \sum_{\substack{m \neq i \\ \beta}} \frac{A^m_\beta A^i_\beta - B^m_{\bar\beta} B^i_{\bar\beta}}{E_m - E_i}\, A^i_\alpha A^m_\alpha + \sum_{\substack{i\alpha \\ E_i>0}} \sum_{\substack{m \neq i \\ \beta}} \frac{A^m_\beta A^i_\beta - B^m_{\bar\beta} B^i_{\bar\beta}}{E_m - E_i}\, B^i_{\bar\alpha} B^m_{\bar\alpha} \right\} \tag{17a}$$

$$\frac{\partial N}{\partial \Delta} = 2\left\{ \sum_{\substack{i\alpha \\ E_i<0}} \sum_{\substack{m \neq i \\ \beta}} \frac{A^m_\beta B^i_{\bar\beta} + B^m_{\bar\beta} A^i_\beta}{E_i - E_m}\, A^i_\alpha A^m_\alpha + \sum_{\substack{i\alpha \\ E_i>0}} \sum_{\substack{m \neq i \\ \beta}} \frac{A^m_\beta B^i_{\bar\beta} + B^m_{\bar\beta} A^i_\beta}{E_i - E_m}\, B^i_{\bar\alpha} B^m_{\bar\alpha} \right\} \tag{17b}$$

Using (14) and (16) it is possible to determine the derivatives $\partial F/\partial\lambda$ and $\partial F/\partial\Delta$ involved in (8)

$$\frac{\partial E}{\partial \lambda} = \sum_{\substack{i\alpha \\ E_i>0}} \sum_{\substack{m \neq i \\ \beta}} \frac{A^m_\beta A^i_\beta - B^m_{\bar\beta} B^i_{\bar\beta}}{E_m - E_i}\, (B^i_{\bar\alpha} A^m_\alpha + A^i_\alpha B^m_{\bar\alpha}) \tag{18a}$$

$$\frac{\partial F}{\partial \Delta} = \sum_{\substack{i\alpha \\ E_i>0}} \sum_{\substack{m \neq i \\ \beta}} \frac{A^m_\beta B^i_{\bar\beta} + B^m_{\bar\beta} A^i_\beta}{E_i - E_m}\, (B^i_{\bar\alpha} A^m_\alpha + A^i_\alpha B^m_{\bar\alpha})\,. \tag{18b}$$

The relations (8), (18) and (17) define the quatitites $\partial N/\partial\lambda$, $\partial N/\partial\Delta$, $\partial G/\partial\lambda$, $\partial G/\partial\Delta$ needed for obtaining changes $\mathrm{d}\lambda$ and $\mathrm{d}\Delta$ from eq. (6).

So the iteration method of solving of the equation (3) consists in the following steps. Firstly, the system (3) is solved with the initial values Δ_0 and λ_0 obtained from the standard model of independent quasiparticles. Obtained in such a way vectors

$(A^i_\alpha, B^i_{\bar{\alpha}})$ are used then for calculation of N and Δ according to (4) and (5). After that the system (6) for changes $d\lambda$ and $d\Delta$ is solved. The systems (3) with new values $\lambda_0 + d\lambda$ and $\Delta_0 + d\Delta$ are solved then again and next iteration can start. The iteration follow one after another until the solutions of (3) converge. Usually two or three iterations were sufficient for obtaining this convergence.

This procedure was applied for increasing rotational frequency Ω (increasing angular momentum). In some value of angular momentum the pairing dissapeared (energy gap Δ became zero) and beyond this value of angular momentum the self-consistency in solving of (3) was performed only through the number of particles. It must be pointed out that we did not search for the precise critical values of angular momentum in which the pairing disappeared. This problem requires the method of projection onto the precise particle number [8].

Since in our approach the nuclear average field is approximated by phenomenological Nilsson hamiltonian involving deformation (see (2)) the system (3) is self-consistent only partially and deformation parameters of average field have to be determined by other way, not from selfconsistency. We use the liquid drop model with inclusion of Strutinsky shell corrections [9] in rotating nucleus for the determination of dependence of deformation on rotational frequency [4]. This method consists in searching for the minimum of the total energy

$$E(\beta, \gamma, \Omega) = E_{\mathrm{LD}}(\beta, \gamma, \Omega) + \delta E_{\mathrm{Strut}} \tag{19}$$

which involves the energy $E_{\mathrm{LD}}(\beta, \gamma, \Omega)$ of rotating charged liquid drop and the shell correction $\delta E_{\mathrm{Strut}} = E_{\mathrm{HFB}} - \tilde{E}_{\mathrm{Strut}}$ where $\tilde{E}_{\mathrm{Strut}}$ is the smoothed Strutinsky energy [9]. The minimization of (19) is performed in the space of deformation parameters β and γ for each value of rotational frequency Ω. The calculation of the total energy of rotating nuclei as a function of its shape was performed by means of the method developed in [4, 5]. The justification of obtained deformation parameters has to be approved by comparison of calculated and theoretical energies of low-lying excitation approved by comparison of calculated and theoretical energies of low-lying excitations.

The calculations of deformation were performed for ^{168}Yb and ^{168}Er. The parameters of singleparticle Nilsson hamiltonian were taken from [21] and pairing strength constants were determined from semiempirical relation

$$G = \left(19.2 \pm 7.4 \frac{N - Z}{A}\right) \frac{1}{A} \text{ MeV}$$

where sign + valids for protons and sign − for neutrons. The equation (3) was solved separately for protons and neutrons and all protons and neutrons shells up to $N = 7$ were involved in calculations. Summation in HFB equations was performed over $2\sqrt{(15\, Z(N))}$ lowest quasiparticle states. Calculation was carried out for 10 different values of Ω in the interval from 0.05 to 0.7 MeV.

Fig. 1 shows the equilibrium deformation of ^{168}Yb as a function of angular

angular momentum (see [10]). For rotational frequency $\Omega \leqq 0.3$ MeV these results can be compared with calculation in refs. [11, 12]. All these calculations forecast the same change of deformation parameters with increasing angular momentum.

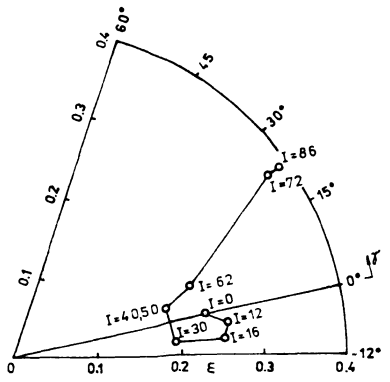

Fig. 1

Equilibrium quadrupole deformation of ^{168}Yb for different values of angular momentum. The deformations corresponding to given value of angular momenta are denoted by points.

The axially deformed nuclei in ground state gains the nonaxial deformation ($\gamma \neq 0$) in the process of rotation. Firstly the parameter γ of nonaxial deformation has the negative values, however in the high spin region corresponding to $\Omega > 0.3$ nonaxiality changes its sign. This demonstrates that inertical properties of nucleus are similar to thats of rigid body.

Some nuclear characteristics determining the energy balance during rotation are presented in fig. 2. The curve denoted by 2 corresponds to the states of yrast line while the curve 1 represents the experimental ground band states. One can see that

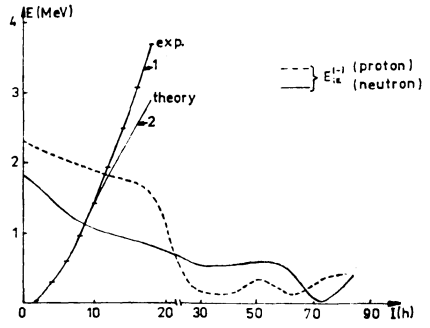

Fig. 2

The calculated and experimental lowest two-quasiparticle energies $E_{ik}^{(-)}$ as a function of angular momentum. Figure contains also calculated and experimental yrast line energies. The both functions are given for ^{168}Yb.

for $I \leqq 12$ the agreement between the theory and experiment is quite satisfactory (calculation does not contain any free parameters) while for higher spins the model overestimates nonadiabatic effects. Calculated nucleus moment of inertia $\Theta = \langle \hat{J}_x \rangle / \Omega$ increas very rapidly in comparison with experimental data. Analogic results were obtained in [4, 37].

The fig. 2 also contains the lowest two-quasiparticle energies $E_{ik}^{(-)} = \min \{E_{ik}, E_{\bar{i}\bar{k}}\}$ for protons and neutrons. In the low spin region ($I \leqq 20$) they lie above 1 MeV. Neutron two-quasiparticle energies keep high values till the higher spins. In the region of spins where $\Delta = 0$ there are no other regularities in dependence of $E_{ik}^{(-)}$ on I.

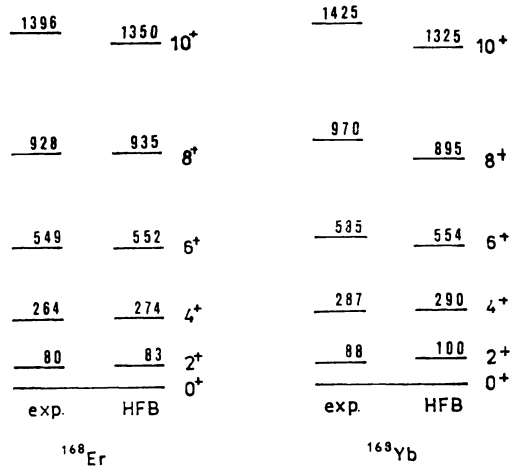

Fig. 3

The comparison of experimental and calculated energies of ground band for ^{168}Er and ^{186}Yb. The values are given in KeV.

The fig. 3 shows the results of calculation of the yrast line states. The agreement of the calculated and experimental values of energies of ground band is satisfactory. Unlike the most of theoretical papers the free parameters were: frequency, energy gap, quadrupole axial deformation ε and nonaxial deformation γ (not only Ω and Δ).

3. Equilibrium characteristics of heated fast rotating nuclei

If excitation energies above yrast line are sufficient for creation of the states involving the large number of particle-hole configurations the description of nuclear properties can be carried out by statistical approaches. In the framework of such approaches the nuclear properties are determined by expectation values of physical observables averaged over the large number of excitation states of the nucleaus. That means the expectation value of the operator $\hat{O}$ is given by

$$\langle \hat{O} \rangle = Sp\{\hat{O} \exp(-\hat{H}/t)\}/Sp\{\exp(-\hat{H}/t)\} \tag{20}$$

where $\hat{H}$ stands for the hamiltonian of the system and the nuclear temperature t characterizes the excitation of nucleus.

The pairing correlations are not discussed in this paper because their role is substantial only in the region of low temperature $t \leqq 0.6$ MeV and low spins $I \leqq \leqq 25-30\,\hbar$. However it has to be noted that the generalization of the model used in this paper for the case of the analysis of the pairing effects in rotating nuclei represents quite complicated problem (see e.g. [13, 14, 15]). The vibrational degrees of freedom of rotating nuclei are not involved in this paper as well. They were discussed in detail in our previous papers [6, 16].

In average field approximation the nucleus hamiltonian $\hat{H}$ involving two-particle effective potential is substituted by one-particle average hamiltonian which can be obtained by selfconsistent way. In rotating frame this average field can be expressed in the form of the sum of one-particle operators (so called routhians) [6, 17].

$$R_{\text{S.p.}} = \frac{p^2}{2m} + V(r) - \Omega j_x \,. \tag{21}$$

In the case of heated fast rotating nucleus it is convenient to introduce the total routhian as a function of deformation parameters ε, γ, rotational frequency Ω and temperature t (see e.g. [18])

$$R(\varepsilon, \gamma, \Omega, t) = E_{\text{LD}}(\varepsilon, \gamma, \Omega = 0) + \sum_{i=1}^{\infty} \varepsilon_i(\varepsilon, \gamma, \Omega)\, \bar{n}_i(t) - \overline{} - \sum_{i=1}^{\infty} \varepsilon_i(\varepsilon, \gamma, \Omega = 0)\, \bar{n}_i(t) \,, \quad t = 0 \,. \tag{22}$$

Here E_{LD} stands for total energy of nonrotating nucleus in the liquid drop model, ε_i are the energies of single-particle states in rotating frame which are defined as eigenvalues of singleparticle routhian

$$R_{\text{S.p.}}(\varepsilon, \gamma, \Omega)\, \Phi_i = \varepsilon_i(\varepsilon, \gamma, \Omega)\, \Phi_i \,. \tag{23}$$

In (22) $n_i(t)$ represents the occupation number of the singleparticle state i in heated nucleus which are given by

$$n_i(t) = \left\{1 + \exp\left[\frac{\varepsilon_i(\varepsilon, \gamma, \Omega) - \lambda}{t}\right]\right\}^{-1} \tag{24}$$

where the Fermi level λ for protons and neutrons is connected with the corresponding number of particles by the following relation

$$\left.\begin{matrix} N \\ Z \end{matrix}\right\} = \sum_i \bar{n}_i \,. \tag{25}$$

The bar above the last term in (22) means the averaging according to shell correction method of Strutinsky [9] in zero temperature. This method is applicable in our case only if the following condition is sutisfied

$$\overline{\sum_i \varepsilon_i(\varepsilon, \gamma, \Omega, t = 0)} - \overline{\sum_i \varepsilon_i(\varepsilon, \gamma, \Omega = 0, t = 0)} \simeq -\tfrac{1}{2}\Omega^3\, \Phi_{\text{R.B.}}(\varepsilon, \gamma) \tag{26}$$

that means if the smooth part of rotation energy of cold nucleus is approximately equal to rotation energy of nucleus taken as rigid body with the same deformation. In such a case the total routhian in zero temperature can be written as follows

$$R(\varepsilon.\,\gamma,\,\Omega,\;t=0)=E_{\mathrm{LD}}(\varepsilon,\,\gamma,\;\Omega=0)-\tfrac{1}{2}\Omega^2\,\Phi_{\mathrm{R.B.}}(\varepsilon,\,\gamma)+\delta S(\varepsilon,\,\gamma,\,\Omega) \tag{27}$$

where the last term represents the shell corrections defined by

$$\delta S(\varepsilon,\,\gamma,\,\Omega)=\sum_{i=1}^{A}\varepsilon_i(\varepsilon,\,\gamma,\,\Omega)-\overline{\sum_{i=1}^{A}\varepsilon_i(\varepsilon,\,\gamma,\,\Omega)}\,. \tag{28}$$

The expression (27) for nonrotating case $\Omega = 0$ is identical with (19). This identity could be expected since the basic assumptions of our approach given in introduction of this paper are the same for cold nucleus as well as for heated nucleus.

The entropy S of heated nucleus and its excitation energy above the yrast line are given by standard formulae [18]

$$S=\sum_i\left[\frac{\varepsilon_i(\beta,\,\gamma,\,\Omega)-\lambda}{t}\,n_i(t)-\ln\left(1-\bar{n}_i(t)\right)\right] \tag{29}$$

$$U=\sum_i\varepsilon_i(\beta,\,\gamma,\,\Omega)\left[\bar{n}_i(t)-\bar{n}_i(t=0)\right]. \tag{30}$$

Cranking model angular momentum of heated nucleus is defined as follows

$$I=\sum_i j_{ii}^{x}\,n_i(t) \tag{31}$$

where single particle matrix elements j_{ii}^{x} are determined in terms of the single particle wave functions Φ_i (see (23)).

The analysis of the properties of excited heated nuclei can be carried out by means of different thermodynamic potentials as a function of corresponding thermodynamic variables. The most convenient ones for nuclear physics are following

i) Gibbs-Routhian function

$$F_{\mathrm{R}}(N,\,\Omega,\,t)=R(N,\,\Omega,\,t)-tS \tag{32}$$

ii) Free energy of Gibbs potential

$$F(N,\,I,\,t)=F_{\mathrm{R}}(N,\,\Omega,\,t)+\Omega I \tag{33}$$

iii) Total energy as a function of entropy

$$E(N,\,S,\,I)=F(N,\,I,\,t)+tS=E(N,\,S=0,\,I)+U(N,\,I) \tag{34}$$

where $E(N,\,0,\,I)$ is the yrast line energy and $U(N,\,I)$ stands for the excitation energy above yrast line for given value I.

The choice of corresponding thermodynamic potential depends on the character of investigated problem. It is evident that all potentials are equivalent from the point of view of studying of equilibrium characteristics and the equilibrium shape of the average field of heated nucleus can be found from extrem condition for arbitrary from these potentials.

Further the results of the calculations of thermodynamic potentials will be presented. These calculations were performed using two types of average field: Nilsson and Wood-Saxon fields and we are restricted ourselves to the following intervals of deformation parameters, temperatures and rotational frequences:

$$0 \leqq \varepsilon \leqq 0.6 \quad \text{for} \quad 0° \leqq \gamma \leqq 60°$$
$$0 \leqq \varepsilon \leqq 0.3 \quad \text{for} \quad -60° \leqq \gamma \leqq 0°$$
$$0 \leqq t \leqq 2 \text{ MeV} \quad \text{for} \quad 0 \leqq \Omega \leqq 1 \text{ MeV}$$

3.1. Results for the Nilsson average field

The method described above was used for determination of equilibrium shapes of fast rotating even-even nuclei in the mass region $60 \leqq Z \leqq 76$, $90 \leqq N \leqq 108$. The average field $V(\vec{r})$ was approximated by Nilsson potential in the form presented in [4]

$$(35) \quad V(\vec{r}) = V_{\text{HO}}(\vec{r}) + V_{\text{Corr}}(\vec{r})$$
$$V_{\text{HO}}(\vec{r}) = \tfrac{1}{2}\hbar\omega_0\varrho^2 \cdot$$
$$\cdot \left[1 - \tfrac{2}{3}\varepsilon\sqrt{\left(\tfrac{4}{5}\right)}\pi\cos\gamma Y_{20} + \tfrac{2}{3}\sqrt{\left(\tfrac{4}{5}\right)}\pi\varepsilon\sqrt{\left(\tfrac{1}{2}\right)}\sin\gamma(Y_{22} + Y_{2-2})\right]$$
$$V_{\text{Corr}}(\vec{r}) = -\varkappa\hbar\mathring{\omega}_0[2\vec{l}\vec{s} + \mu(\vec{l}^2 - N(N+3)]$$

Harmonic oscillator potential V_{HO} depends on two parameters ε and γ of quadrupole deformation which determine the nuclear shape. The term V_{Corr} is introduced to average field in order to improve the description of singleparticle nuclear characteristics and inertial moment of nucleus. It was shown (see e.g. [4]) that moment of inertia calculated from Nilsson potential (35) and averaged by procedure of shell correction method almost coincides with the value obtained for rigid body with the shape. The parameters $\varkappa$ and μ in the term V_{Corr} are chosen in order to reproduce the experimental sequence of singleparticle states for deformed rare-earth nuclei [19]. Oscillator frequency had its standard value $\hbar\omega_0 = 42A^{-2/3}[1 \pm (N-Z)/3A]$ MeV where the upper sign corresponds to neutrons and lower to protons.

Fig. 4 presents the dependence of free-energy minimum in the space of deformation parameters ε and γ on angular momentum for ^{152}Sm, ^{160}Yb and ^{180}Os. The calculations were carried out for nuclear temperature $t = 0.2$ MeV. The excitation energy U corresponding to this temperature is $U \sim 0.5$ MeV. Such value of the temperature and excitation energy does not destroy the shell-effects and, at the same time, facilitates the interpolation procedure used in the calculations. The comparison of fig. 4 with the similar hodographs in [4] (see figs. 19, 21 in [4]) shows the good agreement between the approaches used in this paper and that in [4]. In both approaches the equilibrium deformation parameter γ is small and negative in ^{152}Sm for angular momentum $0 \leqq I \leqq 30$ and both the papers give the same value of angular momentum for which the nucleus ^{152}Sm reaches the oblate shape (deformation $\gamma = \pi/3$).

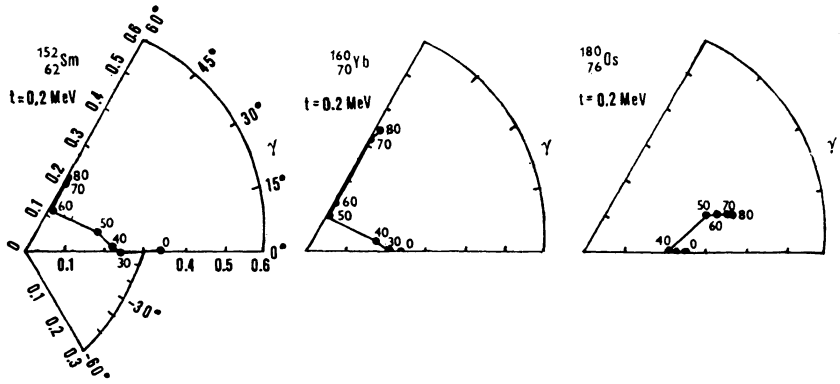

Fig. 4

The hodographs of equilibrium deformation parameters for different angular momenta in (ε, γ) space obtained from condition of minimum of free energy $F(\varepsilon, \gamma, I, t)$ for $t = 0.2$ MeV for ^{152}Sm, ^{160}Yb and ^{180}Os. The points in figs. correspond to written value of angular momentum.

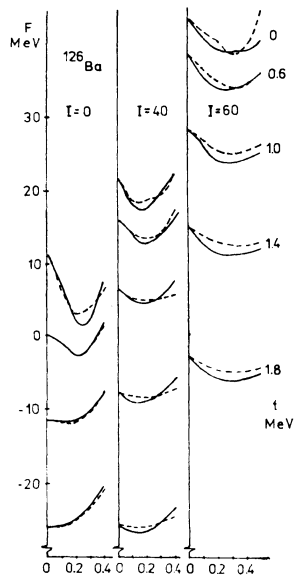

Fig. 5

The dependence of free energy of ^{126}Ba on axial deformatien for different temperature. Full lines correspond to oblate shape and to angular momentum directed along the symmetry axis. Dotted curves are connected with collective rotation of nucleus with prolate shape.

Fig. 5 shows the free-energy F of ^{126}Ba as a function of deformation parameters for different temperatures t. There are presented only the sections of the surface of F along the axial-symmetry axes of prolate ($\gamma = 0°$) or oblate ($\gamma = \pi/3$) ellipsoid.

The smoothing of shell effects with increasing temperature can be seen from figs. 6

and 7 where the Gibbs-Routhian function F_R and dynamic moment of inertia $\mathcal{J} = \langle I_x \rangle / \Omega$ are demonstrated as a functions of deformation for different values of temperature t and rotational frequency Ω. The equilibrium shape becomes spherical

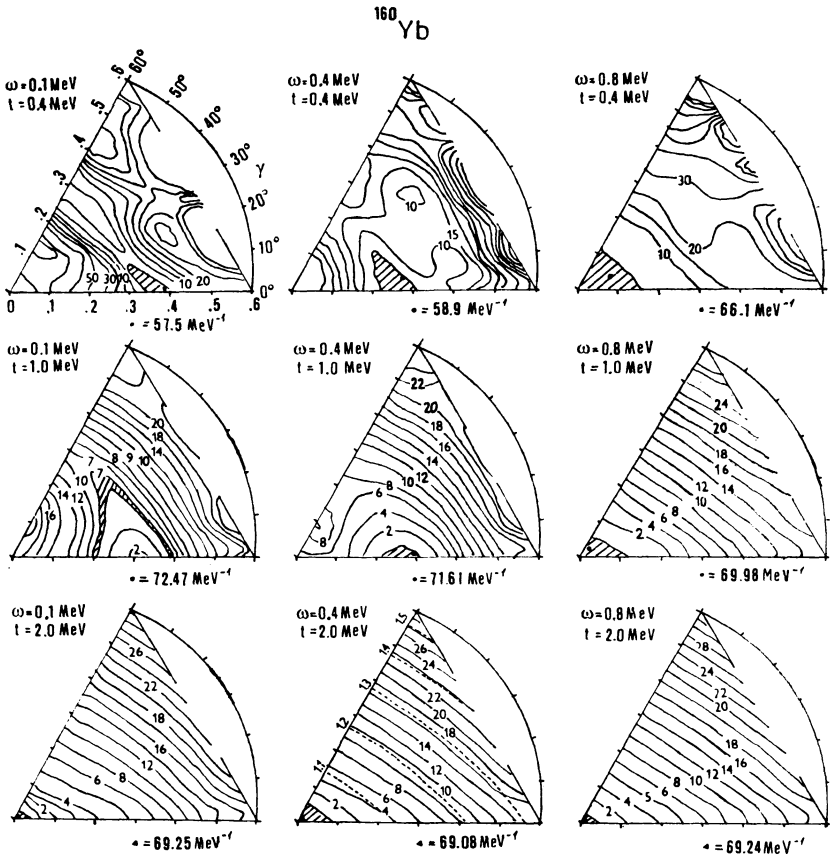

Fig. 6

Gibbs-Routhian function F_R surfaces for different rotation frequences $\Omega = \omega$ and temperature t for ^{160}Yb. The minimum value of F_R for given value of Ω and t is shown under the corresponding figure. The marked region in the vicinity of F_R^{min} contains the points which differ no more than by 0.5 MeV from F_R^{min}. The lines of fixed value of F_R are characterized by numbers. If one adds numbers to F_R^{min} it is possible to obtain the value of F_R corresponding to given equipotential curve.

for $\Omega = 0$ when temperature reaches high values while fast rotation gives raise to the oblate deformation with symmetry axis in direction of angular momentum. The curves of fixed value of F_R for $t = 2.0$ MeV behave similarly to those predicted by liquid drop model. The inertia moment oscillates for two values of temperature but it depends on deformation in the same way as in liquid drop model for high temperatures $t \sim 2.0$ MeV. In segment corresponding to $\Omega = 0.4$ MeV and $t = 2.0$ MeV

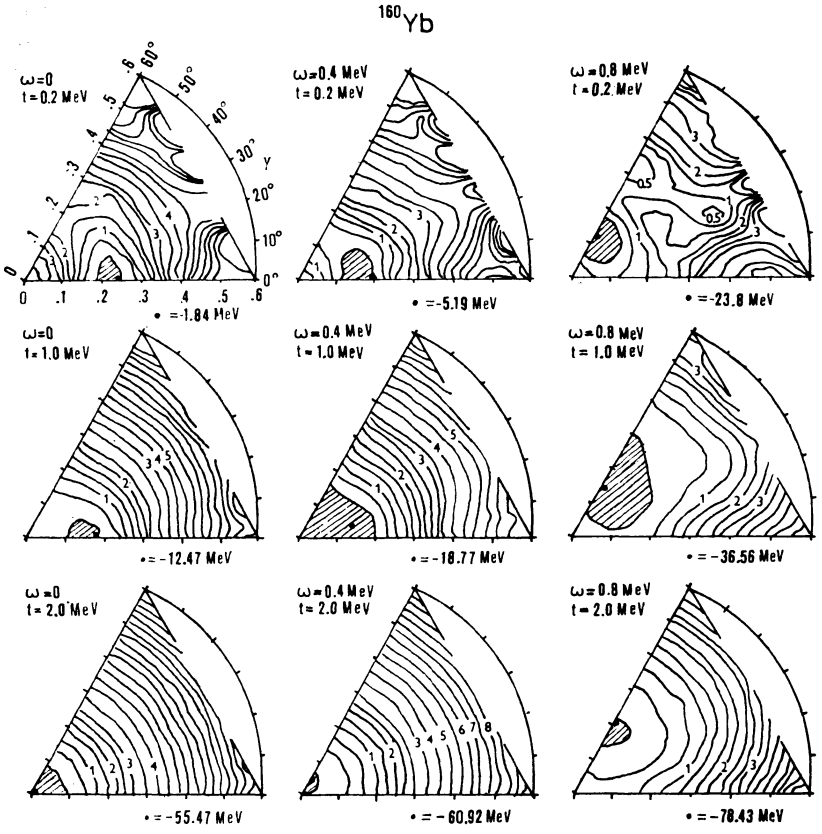

Fig. 7

The dynamical moment of inertie surfaces ($\mathcal{J}(\varepsilon, \gamma) = \langle I \rangle / \Omega$) for different values of $\Omega = \omega$ and t. The minimal values $\mathcal{J}^{\min}_{(\varepsilon,\gamma)}$ are denoted by points in each figure and their numerical values are under each figure. The numbers for equipotential curves determine the values of $\mathcal{J}(\varepsilon, \gamma)$ of each curve with respect to $\mathcal{J}^{\min}_{(\varepsilon,\gamma)}$.

in fig. 11 there are the lines of fixed value of the quantity $f(\varepsilon, \gamma)$ defined as

$$f(\varepsilon, \gamma) = \frac{\mathcal{J}_{\text{R.B.}}(\varepsilon, \gamma)}{\mathcal{J}_{\text{R.B.}}(0,0)} = (1 + \tfrac{2}{3}\varepsilon \sin(\gamma + 30°))(1 + \tfrac{8}{27}\varepsilon^2) \tag{36}$$

where $\mathcal{J}_{\text{R.B.}}(\varepsilon, \gamma)$ is the largest from the rigid body moments of inertia. Standard deviation of calculated inertia moment from $\mathcal{J}_{\text{R.B.}}(\varepsilon, \gamma)$ for $t = 2.0$ MeV does not exceed 2% for all values of Ω. The rigid body estimate of the moment of inertia $\mathcal{J}_{\text{R.B.}}(0, 0) = \frac{2}{5}MR_0^2A = 65\ \text{MeV}^{-1}$ ($R_0 = 1.2\, A^{1/3} fm$, M is nucleon mass) is quite close the expectation value $\mathcal{J}(\varepsilon, \gamma)/f(\varepsilon, \gamma) = 66\ \text{MeV}^{-1}$. It must be noted that the function $\mathcal{J}(\varepsilon, \gamma)/f(\varepsilon, \gamma)$ decreases by about 3–4% when ε increases from 0 to 0.6. It can be a cause why the equilibrium deformation point of ^{160}Yb for $t = 2$ MeV and

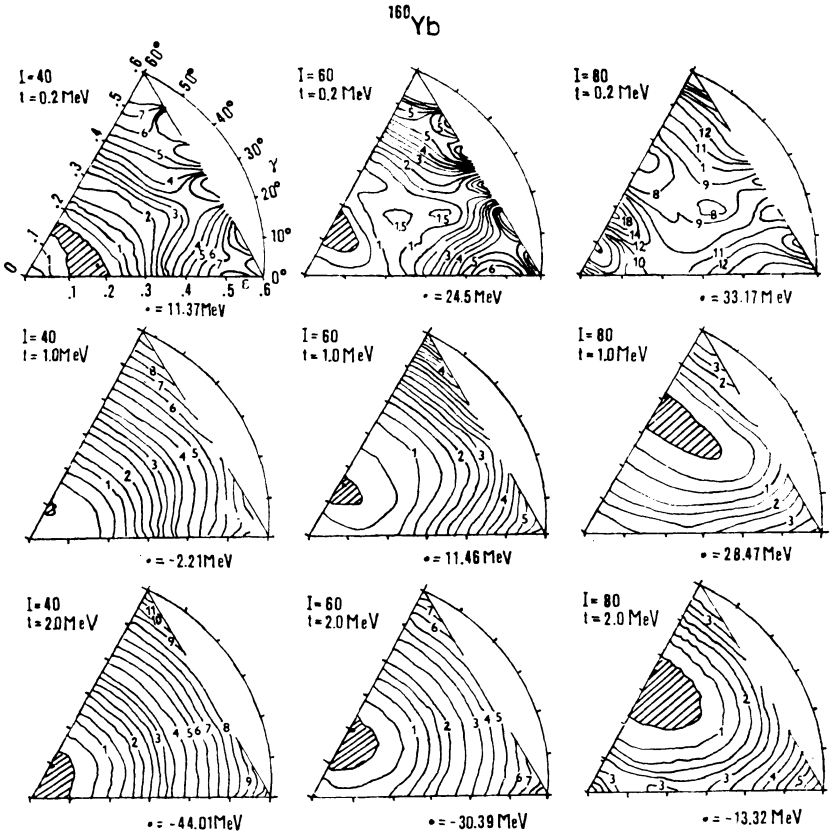

Fig. 8

The total free energy F equipotential curves for different values of angular momentum I and temperature t for ^{160}Yb. The minimum values F^{min} are denoted by points surrounded by marked region. Corresponding values of F^{min} are given under The each figure. The scale of values of F is characterised by numbers for some equipotential curves.

$I = 80$ still remains to be placed on symmetry axis, what is in contradiction with the results of liquid drop model. The second cause of this fact is the neglecting of the higher order of deformation (other than quadrupole) in our calculations.

We will demonstrate obtained results of thermodynamic potentials $F_R(\varepsilon, \gamma, \Omega, t)$, $F(\varepsilon, \gamma, \Omega, t)$ and $E(\varepsilon, \gamma, I, t)$ for the case of typical rare-earth nucleus such as ^{160}Yb. These results are presented in the figs 6, 8, 9. The functions $F_R(\varepsilon, \gamma, \Omega, t)$, $F(\varepsilon, \gamma, I, t)$ and $E(\varepsilon, \gamma, I, S)$ determine the potential surface of rotating nuclei. From the mathematical point of view the Gibbs-Routhian function $F_R(\varepsilon, \gamma, \Omega, t)$ is the simplest. However the variables Ω and t are not measurable quantities. They represent formal mathematical variables (Lagrange multipliers) which were introduced in order to avoid the difficulties in solving of variation problem with additional conditions. On

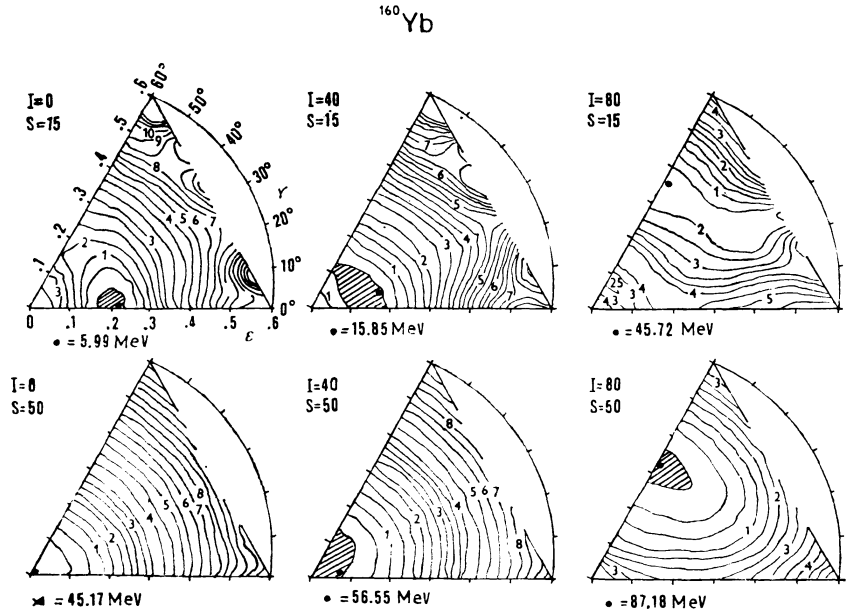

Fig. 9

The total energy $E(\varepsilon, \gamma; I, S)$ surfaces for different values of angular momentum I and entropy S for ^{160}Yb. The points surrounded by marked region corresponds to minima of energy for given I and S. The corresponding values of E^{min} are given under the each figure. The scale of values of E is characterised by numbers for some equipotential curves.

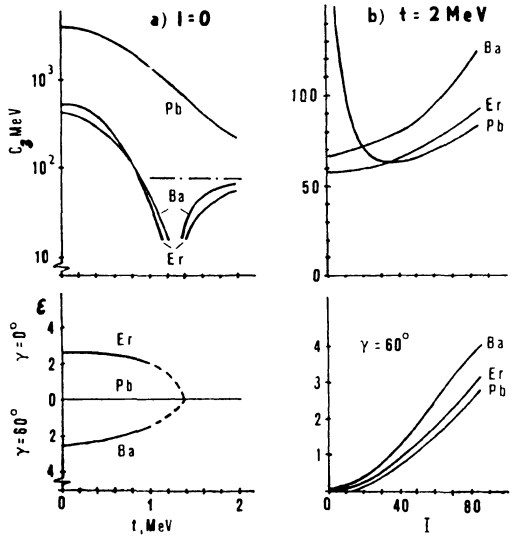

Fig. 10

Temperature dependence of rigidity and equilibrium axial deformation for ^{126}Ba, ^{160}Er, ^{208}Pb for zero angular momentum (a) and dependence of these quantities on I for $t = 2$ MeV (b).

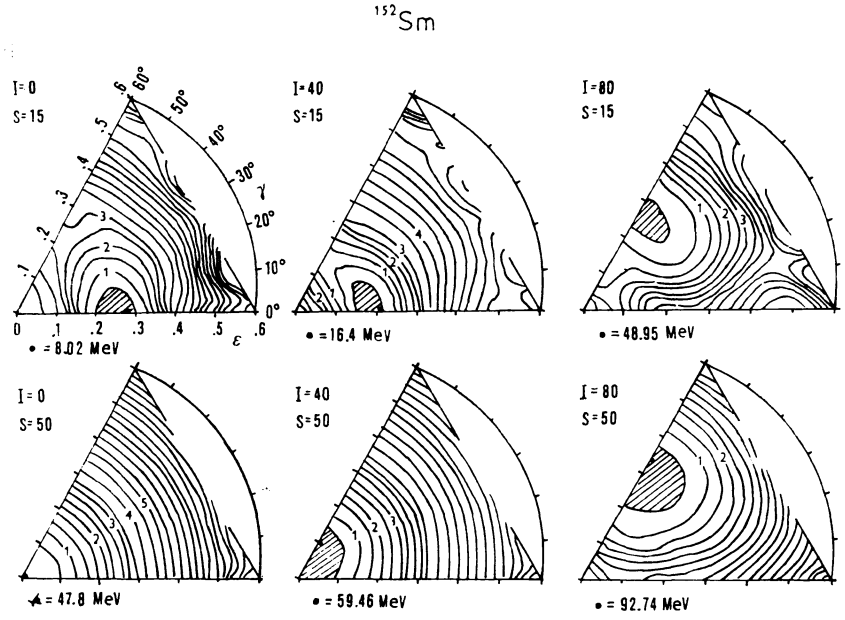

Fig. 11

The total energy $E(\varepsilon, \gamma, I, S)$ surfaces for different values of angular momentum I and S for ^{152}Sm. The description of figure is the same as in fig. 9.

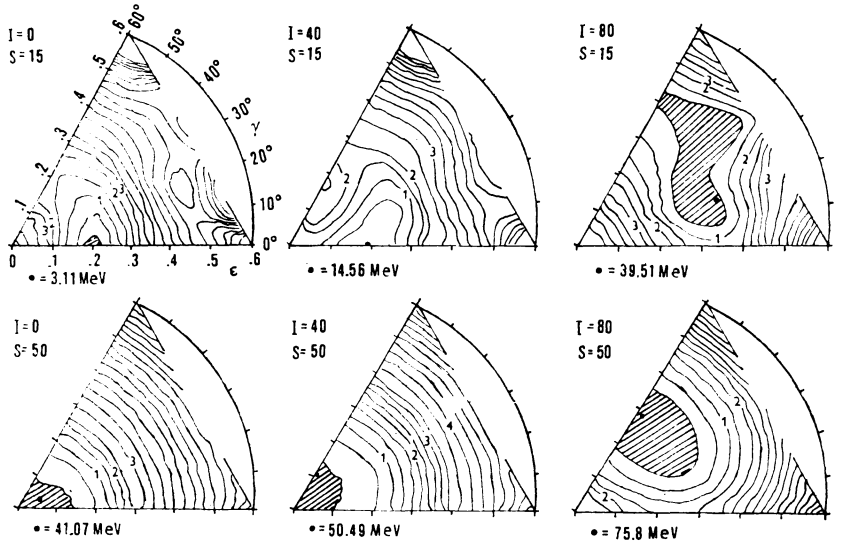

Fig. 12

The total energy $E(\varepsilon, \gamma; I, S)$ surfaces for different values of angular momentum I and S for ^{180}Os. The description of figure is the same as in fig. 9.

the other hand the calculation of F and E requires the interpolation procedure in transition from frequency Ω to given value I of angular momentum and from temperature t to given value S of entropy.

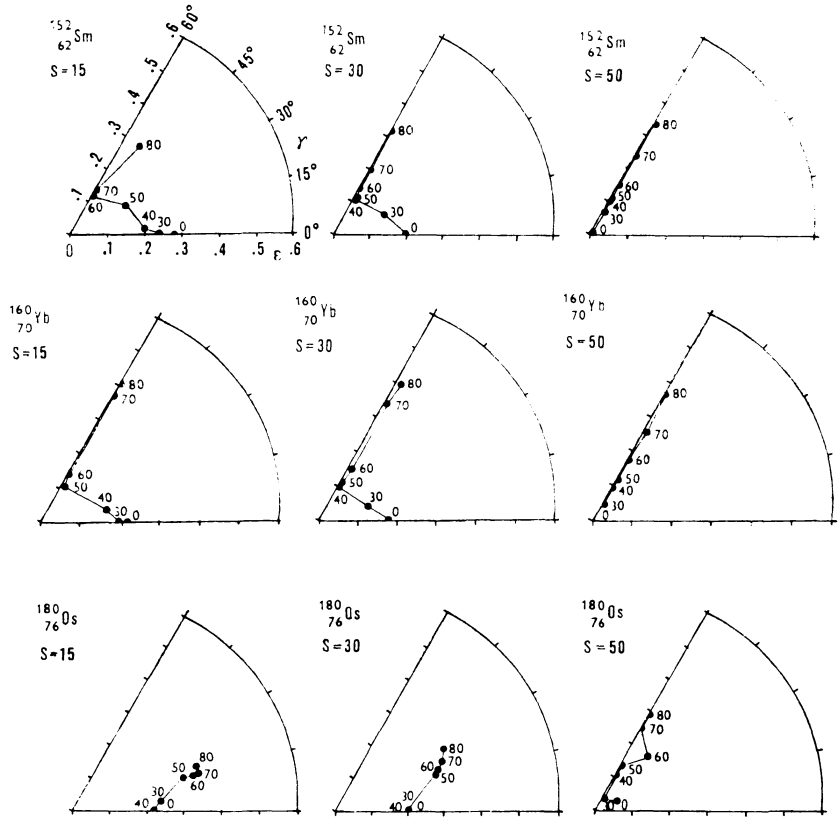

Fig. 13

The hodographs of minimal energies $E(\varepsilon, \gamma; I, S)$ for different values of entropy $S = 15, 30, 50$ for ^{152}Sm, ^{160}Yb, ^{180}Os. The points in hodographs correspond to given values of angular momentum.

If the variables Ω, t and I, S are connected by the expression (29) and (31) the function $F_R(\varepsilon, \gamma)$, $F(\varepsilon, \gamma)$, $E(\varepsilon, \gamma)$ have to have the common points of minimum in the ε, γ plane. This point determine the equilibrium deformation of nucleus. The density of equipotential curves in the vicinity of equilibrium points allows to estimate the forces making for the equilibrium position of nuclear shape. One can see from the figs 10–13 that in low temperature region the equilibrium deformation is fully determined by shell correction. The nucleus ^{160}Yb is prolate for low $\Omega(I)$ and small excitation energy ($\varepsilon \sim 0.24$, $\gamma = 0°$ for $\Omega = I = S = 0$) while the fast rotation ($\Omega \geqq 0.5$ MeV, $I \geqq 30$) leads to the nonstability of prolate configuration even for

low temperature. For higher rotational frequency $\Omega \geqq 0.7$ MeV ($I \geqq 50$) the nucleus ^{160}Yb obtained the oblate shape with symmetry axis in the direction of angular momentum. The further increasing of Ω brings about the large value of ε and strong centrifugal forces what demonstrates the increasing role of liquid drop component of energy.

Statistical excitations which are characterized by participation of a large number of degrees of freedom and introduction of nuclear temperature t decrease the shell correction in energy. With increasing nuclear temperature t the transition from shell regime of rotation to liquid drop one occurs for lower values of momenta I. For $t \geqq 1.0-1.2$ MeV ($U \geqq 14-17$ MeV) the prolate configuration in ^{160}Yb is nonstable for all values of spin. Character of deformation in this temperature is qualitatively identical with that of rotating drop. For $t \geqq 2$ MeV ($U \geqq 50$ MeV) the shell effects have no influence on nuclear shape.

Fig. 10 demonstrates the behaviour of the most probable deformation of heated nucleus and its rigideness characterized by parameter

$$C = \frac{\partial^2 F}{\partial \varepsilon \partial \gamma}$$

as a function of angular momentum I and temperature t for some typical nuclei from the region $100 \leqq A \leqq 210$. The results show the basic details of evolution of the nuclear properties in the process of heating. This picture confirms again the fact of lowering of shell effects with increasing temperature. For $t \sim 1.2$ MeV and $0 \leqq \varepsilon \leqq \varepsilon_{\text{equil.}}(t = 0)$ the deformation variation of liquid drop component of energy is approximately equal to variation of shell component of energy. The figs. 6, 7, 9 give the explanation. One can see from fig. 9 the energy surface $E(\varepsilon, \gamma)$ has small minimum for $I = 0$, $S = 50$. The analogous situation is observed for $F_{\text{R}}(\varepsilon, \gamma)$ (fig. 6) and $F(\varepsilon, \gamma)$ (fig. 8). This reflects the transition from deformation typical for shell model to liquid drop model deformation which is clearly spherical for $I = 0$, $S = 50$.

The calculations with result given in figs. 6–10 allow to derive the interpolation formula which connects the angular momenta I and excitation energies U for which the transition from shell regime of deformation to liquid drop one occurs

$$(I/I_n)^2 + (U/U_n)^2 \approx 1 \,. \tag{37}$$

In the case of ^{160}Yb $I_n \approx 40$, $U_n \approx 15$ MeV. For I and U satisfying (37) the deformation variation of shell component and liquid drop component of corresponding thermodynamical potentials are equal each other. The expression (37) represents the equation of closed curve in the space of I, U. Inside this curve the shell correction part of energy dominates while outside region prefers the liquid drop part of energy.

The authors of [4] pointed out that rotation can lead to the preference of energy minimum of shell energy for high values of ε. Our results for ^{160}Yb for $t = 0$ show the decreasing of F_{R}, F, E leading to the second minimum for $\varepsilon > 0.6$. This minima can be distinguished well also for $U \sim 5$ MeV ($t \sim 0.5$ MeV, $S \sim 15$) but they are

completely gone away for $U \sim 15$ MeV ($t \sim 1.0$ MeV, $S \sim 30$). One can conclude from this that the value $U \sim 15$ MeV is the critical value for which the transition from shell regime rotation to the liquid drop one occurs for all investigated cases of deformation.

The figs. 11 and 12 demonstrate the minimum value of $E(\varepsilon, \gamma)$ for the other nuclei ^{152}Sm and ^{180}Os of rare-earth region. These figs. confirm the conclusion about regime transition given above for ^{160}Yb. The potential surfaces for different nuclei are quite different for low values of temperature and entropy and therefore the hodographs of minimum energy for small t or S or U differ considerably in fig. 13. However not so high excitation ($t \sim 1.0$ MeV, $S \sim 30.0$, $U \sim 15.0$ MeV) cancels these differences and higher excitation leads to the liquid drop mechanism of evolution of nuclear shape in rotation.

3.2. Results of calculation with Saxon-Woods average field

In this part of paper the dependence of termodynamical potentials and energy on nuclear deformation is investigated, concretely the evolution of this dependence in the process of nuclear rotation. In opposite to previous part 3.1 the nuclear average field is approximated by Saxon-Woods singleparticle potential

$$V^{(n)}(\vec{r}; \beta) = V^{(n)}_{\text{cent}}(\vec{r}; \beta) + V^{(n)}_{\text{ls}}(\vec{r}; \beta) \tag{38a}$$

$$V^{(p)}(\vec{r}; \beta) = V^{(p)}_{\text{cent}}(\vec{r}; \beta) + V^{(p)}_{\text{ls}}(\vec{r}; \beta) + V_{\text{Coul}}(\vec{r}; \beta) \tag{38b}$$

Here $V_{\text{cent}}(\vec{r}; \beta)$ is the central part of the average nuclear field, V_{ls} stands for the spin-orbital potential and V_{Coul} represents the Coulomb potential of homogeneously charged part of space contained in nuclear surface. Central part V_{cent} is given by

$$C_{\text{cent}}(\vec{r}; \beta) = -V_0/[1 + e^{(d(\vec{r}, \beta))/a}] \tag{39}$$

where V_0 is the potential well depth, $d(\vec{r}, \beta)$ is the shortest distance between the point $\vec{r}$ and nuclear surface and a is the diffuseness parameter of the potential on the nuclear surface. The symbol β characterizes the set of deformation parameters ($\beta \equiv (\beta_2, \beta_4, \gamma)$). We use the Bohr parametrization of quadrupole deformation

$$\beta_{20} = \beta_2 \cos \gamma \tag{40}$$

$$\beta_{22} = \beta_{2-2} = \frac{1}{\sqrt{2}} \beta_2 \sin \gamma$$

where γ characterizes the nonaxial deformation. It is assumed that hexadecapole degrees of freedom does not violate the symmetry of quadrupole deformation. By other words it means that the quadrupole and hexadecapole degrees of freedom have the same symmetry axis in the transition from $\gamma = 0°$ to $\gamma = n \cdot 60°$ ($n = \pm 1, \pm 2, \pm 3$). This leads to the three independent ways of the parametrization of hexadecapole degrees of freedom. One of them used in this paper has the fol-

lowing form

$$\beta_{40} = \frac{\beta_4}{6}(5\cos^2\gamma + 1)$$

$$\beta_{42} = \beta_{4-2} = \frac{\beta_4}{6}\sqrt{\frac{15}{2}}\sin 2\gamma \tag{41}$$

$$\beta_{44} = \beta_{4-4} = \frac{\beta_4}{6}\sqrt{\frac{35}{2}}\sin^2\gamma$$

where β_4 is the parameter determining the value of the hexadecapole deformation.

The spin-orbital potential has its standard form

$$V_{ls}(\vec{r};\beta) = -\lambda\left(\frac{\hbar}{2Mc}\right)^2(\vec{\nabla}V_{cent}(\vec{r};\beta)(\vec{\sigma}\times\vec{p})) \tag{42}$$

where $\vec{p}$ and $\vec{s} = \vec{\sigma}/2$ are nucleon momentum and spin operators respectively, and $V_{cent}(\vec{r}, \beta)$ is given by eq. (39) with corresponding parameters. The parameters of the central as well as spin-orbit parts of potential were taken from [21]. The Coulomb potential for protons has been determined as a classical electrostatic potential of

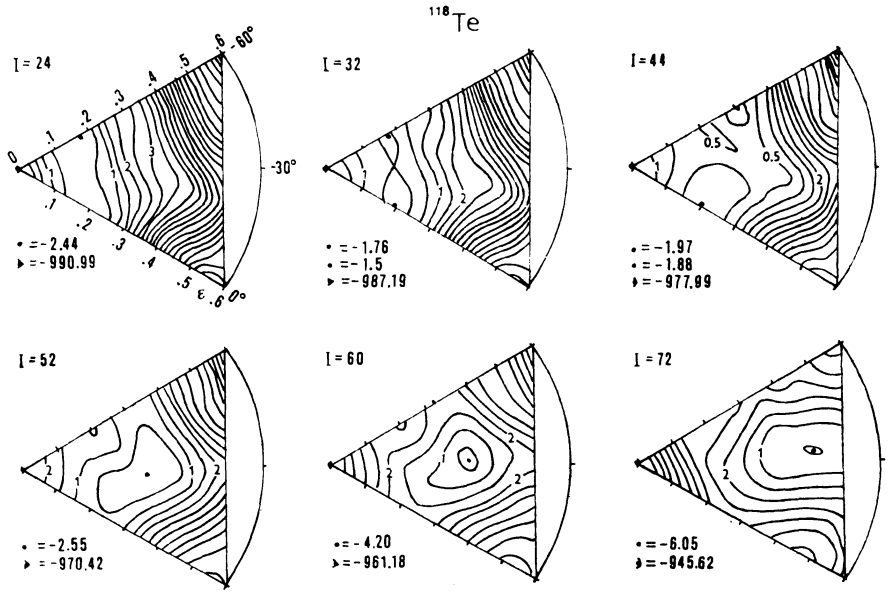

Fig. 14

The equipotential surfaces of Gibbs function $F(\beta, \gamma; I, t)$ for different values of angular momentum I and temperature $t = 0.2$ MeV for ^{118}Te. The points correspond to the minimum of free energy $F_{min} = F(\beta = \gamma = 0) + \Delta F(\beta, \gamma_{min})$ (corresponding values $F(0, 0)$ and ΔF_{min} are given under the each surface). The numbers for some equipotential curve determine the scale of changing of free energy, for instance the curve with number 2 corresponds to value $F = F_{min} + 2$ MeV.

a uniformly charged nucleus with a nuclear surface characterised by deformation parameter β.

Fig. 14 shows the equipotential curves of free energy for ^{118}Te in dependence on deformation. It can be seen that this nucleus is sufficiently soft with respect to nonaxial

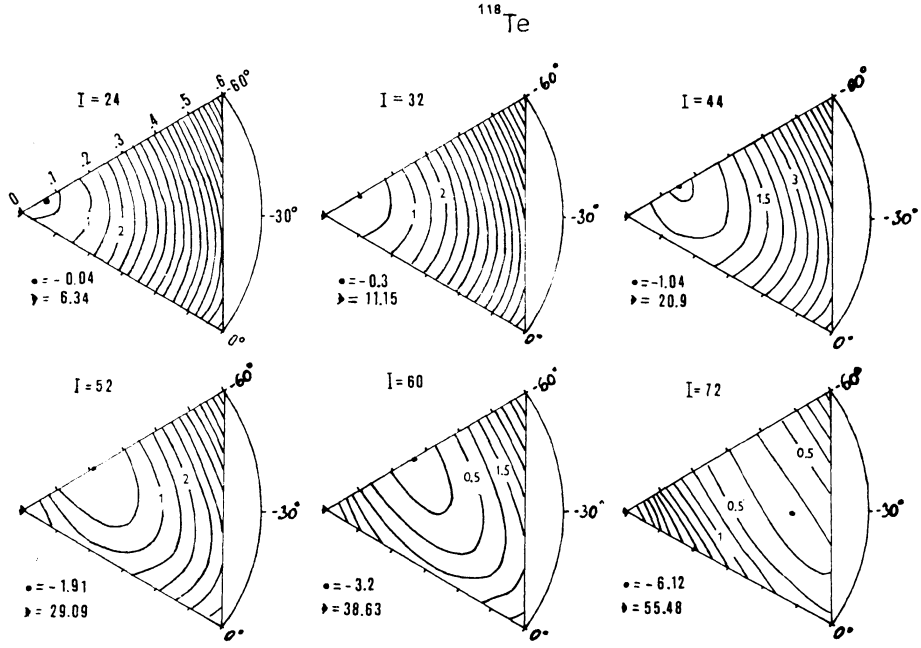

Fig. 15

The equipotential surfaces of liquid drop component of deformation energy for different values of I for ^{118}Te. The description of figure is the same as in the fig. 14.

deformation. The analysis of liquid drop component energy of deformation ^{118}Te (see fig. 15) confirms the increasing of axial deformation β_2 with growing of angular momentum. This fact can be cleared up by means of lowering of shell-effects. The analogous result was obtained in [22].

The yrast line of ^{118}Te is formed by three rotational bands (see fig. 16). In low-spin region ($I < 30\ \hbar$) the yrast ine is represented by ground rotational band characterized by axially oblate shape ($\gamma = \pm 60$). This deformation is determined by shell correction part of total energy which is decisive in this region of spins. For higher spins ($I > 30\ \hbar$) the shell corrctions prefer the axially prolate shape ($\gamma = 0°$) which corresponds to the second band in fig. 16. The third band is connected with nonaxial shape which characterise ^{118}Te for high spins $I > 44\ \hbar$. The analogous predictions can be obtained in the case of calculation based on the Nilsson potential [38].

The interesting results was obtained for the nucleus ^{130}Ba. For momentum $I =$ $= 48\ \hbar$ (fig. 17) the shell effects leads to the appearance of two minima in energy

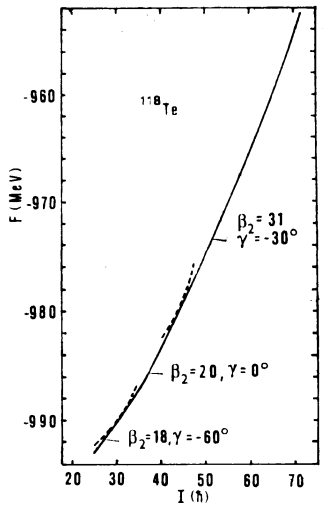

Fig. 16
The yrast line of ^{118}Te.

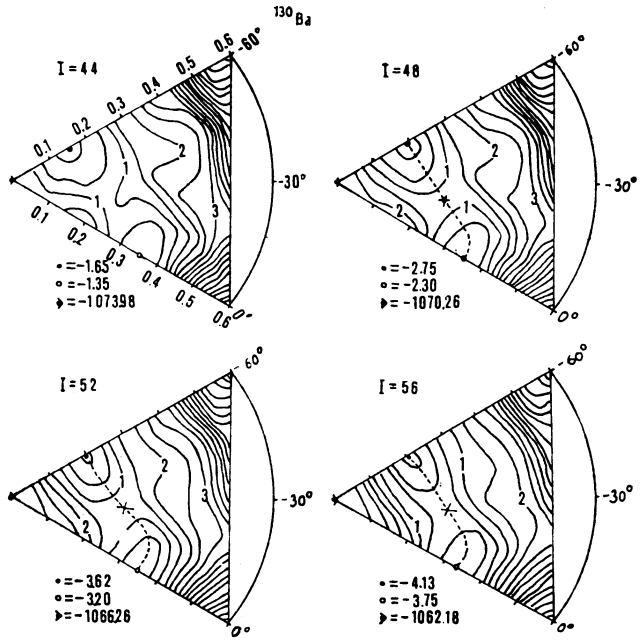

Fig. 17
The free energy equipotential surfaces for different values of I and $t = 0.2$ MeV for ^{130}Be. The description of figure is the same as in the fig. 14.

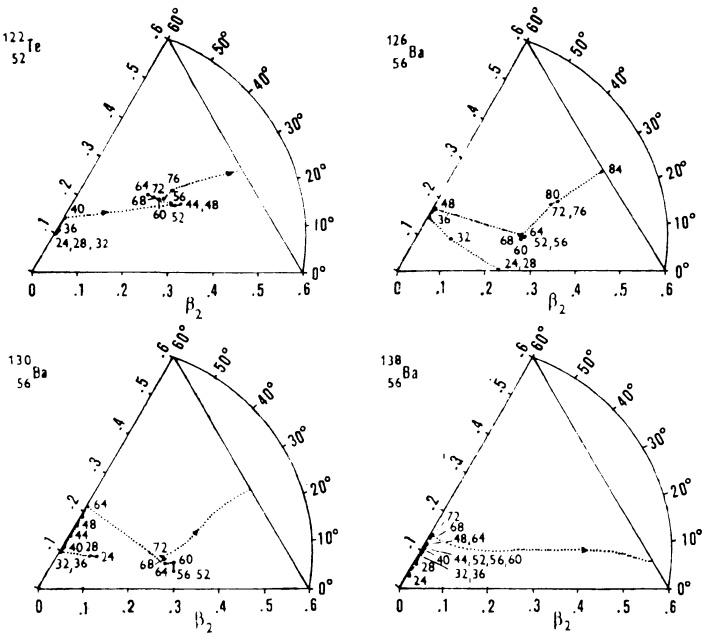

Fig. 18

The free energy hodographs $F(\beta, \gamma; I, t = 0.2\ \text{MeV})$ for ^{122}Te, ^{126,130,138}Be. The points in each hodograph correspond to the minima of free energy for given value of angular momentum.

surface with approximately equal depths. One of them corresponds to axially-oblate shape ($\beta_2 = 0.2$, $\gamma = -60°$) and the second one to axially-prolate shape ($\beta_2 = 0.3$, $\gamma = 0°$). The barier between them seems to be sufficiently high ($\sim$1 MeV) in order to interpretate these states as shape isomers of given nucleus. The barier height diminishes to 0.5 MeV for $I \sim 60\ \hbar$ and further increase of I leads to the axially-prolate shape.

The calculations showed that the change of the shape caused by the rotation of the nucleus with nonoccupied neutron shell $N \sim 70$ and with proton number $Z \geqq 56$ has the special characteristics similar to those of nuclei from rare-earth region $150 < A < 190$. For angular momenta $I \sim 20-30\ \hbar$ the axially-prolate shape ($\gamma = 0°$) with deformation $\beta_2 \sim 0.2$ is the most probable from the point of view of energy. If the angular momentum increases the nucleus becomes more and more unstable with respect to nonaxial deformation. Besides that the liquid drop contribution to deformation energy plays bigger and bigger role so the liquid drop component is comparable with the shell correction component. If angular momentum or rotational velocity is further increased the axial-oblate shape ($\gamma = -60°$) with small deformation $\beta_2 \sim 0.15$ is preferable. Further increase of rotational frequency leads to triaxial deformation ($\beta_2 \approx 0.4$, $\gamma \approx 15°-20°$).

A little difference in behaviour can be observed for nuclei with neutron number

close to magic $N \sim 82$. The shape of this type nuclei is approximately spherical for small angular momenta. Faster rotation leads to the oblate shape with small angular momenta. This shape is favourable up to $I \sim 60-70\,\hbar$. The increase of angular momentum to these values is only accompanied by small growth of β_2. After reaching $I \sim 60-70\,\hbar$ the sharp transition to rotation characterized by axial prolate shape ($\gamma = 0°$) occurs. Just then the deformation β_2 increases to 0.6.

The increase of excitation energy above the yrast line leads to the weakening of shell effects and, as a result of this, to the smoothing of the relief of deformation energy surfaces in $\beta_2 - \gamma$ plane. The characteristic temperature for which the shell correction practically does not influence the deformation is $t \sim 1.1$ MeV. This value was confirmed by calculation with modified Nilsson potential. Therefore this characteristic temperature of 1.1 MeV is probably common for all potentials describing the singleparticle density distribution in the vicinity of Fermi level. The temperatures higher then this characteristic value correspond to rigid-body regime of rotation. It must be noted that inclusion of hexadecapole deformation to the calculations leads to the nonaxial shapes of nuclei for very fast rotation in contradiction to the results obtained for Nilsson average field (see sect. 3.1) where the energy minimum corresponded to axial-oblate shapes for $I \sim 70-80\,\hbar$.

3.3. The results of shape calculation

One of the most important conclusions which can be drawn from the results of calculations presented in previous parts of this paper concerns the determination of critical nuclear temperature $t_n = 1.0-1.2$ MeV ($U_n = 14-17$ MeV) characteristic for disappearance of shell effects in determination of the shape of rotating nuclei. In connection with this conclusion one has to mention two circumstances.

Firstly, it is interesting to compare the value t_n with the predictions of this quantity based on the simple model of energy dependence of the density of single particle states [23]

$$g(\varepsilon) = g_0 + f\cos\left(2\pi\,\frac{\varepsilon - \varepsilon_0}{\hbar\omega_0}\right).$$

The oscillating part of $g(\varepsilon)$ leads to the shell correction in energy of heated magic nuclei

$$U = -\frac{f}{4\pi^2}(\hbar\omega_0)^2\,\tau^2\,\frac{\operatorname{ch}\tau}{(\operatorname{sh}\tau)^2} \tag{43}$$

where

$$\tau = \frac{2\pi^2 t}{\hbar\omega_0} = 2.26\left(\frac{A}{170}\right)^{1/3} t\,. \tag{44}$$

One can see from (43) and (44) that characteristic nucleus temperature for damping of shell effects is higher than our result. It must be however mentioned that our

calculations were performed for deformed nuclei including many nucleons in open shells. In the lowest order in ε deformation does not influence the singleparticle state density fluctuation connecting with the existence of principal shells (see expr. (6.514) in [23]). The deformation enters the thermodynamic potentials through the higher harmonics in Fourier expansion for density of singleparticle states. These higher harmonics do not participate in the expressions for $g(\varepsilon)$ given above. Therefore the damping of shell effects can be expected for lower temperature t than predictions obtained from expressions (43) and (44). The other confirmation of our value t_n is given by different character of the competition between the liquid drop and shell regimes of deformation in spherical and deformed nuclei. The fig. 10 demonstrates this fact. In deformed nuclei ^{126}Ba and ^{160}Er the shell effects disappear very quickly for $t \sim 1.2$ MeV. In opposite to this spherical nucleus ^{208}Pb is characterised by considerable shell effects up to the higher temperatures in comparison with deformed nuclei. The transition from shell regime to liquid drop regime of rotation has the character of phase transition for deformed nuclei while for spherical nucleus ^{208}Pb this transition is slow and smooth.

The second circumstance concerning the critical nuclear temperature t_n is connected with data obtained from (HI, xn) reactions. The typical excitation energy of compound nucleus reached in heavy ion reactions is 20—30 MeV. The shell effects cannot influence the equilibrium deformation of such states. Therefore the liquid drop model calculations can be applied for the analysis of the properties of the states of compound nucleus formed in (HI, xn) reactions such as the critical angular momentum for fission of compound nucleus or fission barier [20]. It must be reminded that the analysis of liquid drop part of energy done in this paper is not comparable with the numerical analysis of fission barier presented in [20, 4]. As it was mentioned in [5] the inclusion of shell corrections can lead to the increase of limitting angular momontum of nucleus settled on the barier by about 30 $\hbar$. However the analysis of experimental data [24] presented by A. Bohr [3] does not confirm this fact. On the contrary it supports our conclusion about the liquid drop model evolution of nuclear deformation for such high excitations.

The first stage of deexcitation of compound nucleus formed in (HI, xn) reaction is accompanied by emmision of nucleons. In such a way the nucleus loses the energy and after reaching the excitation about 10 MeV the deexctiation goes exclusively through the emmision of gamma quanta. According to our calculations the excitation energy about 10 MeV is characterized by large fluctuation of nuclear shape which leads to the collective quadrupole transitions from these states. Our calculation allows one to expect the further deexcitation by gammas which take away the angular momentum keeping the nucleus excited above the yrast line. The shell effects remain still weak in this region of excitations. They become substantial when the excitation energy reduced approximately to 5 MeV above the yrast line (what corresponds to temperatures $t \leqq 0.6$ MeV). Then the nucleus starts to move along the valleys of the shell potential energy surface during the deexcitation in the process of nucleus rota-

rotation. The shell inhomogenities in single particle spectrum play the substantial role in this stage of deexcitation. This shell correction influence concerns not only the statistical characteristics of fast rotating nuclei but also the transition probabilities. Generally speaking the method of calculation of thermodynamic potentials allows to obtain the densities of level for all possible deexcitation channels of decay of compound nucleus formed in heavy ion reactions.

In the end of this part one has to mention that the obtained above basic laws in shape evolution of fast rotating nuclei are independent on the fact if the nuclar average field is approximated by Saxon-Woods or Nilsson potential.

4. Spectrum of quadrupole gamma quanta emmited by fast rotating nuclei

Though the gamma spectrum emmited from high excited fast rotating nucleus is complex its basic characteristics can be cleared up in terms of the analysis of shape evolution. Particularly in this part of paper it is shown that the irregularities of gamma spectrum from deexcitation of high spin states of ^{118}Te [25] can be explained by changes in shape of this nucleus in the process of its rotation.

We will assume that the main contribution to the gamma spectrum comes from the quadrupole transitions between the states of yrast line or the states of rotational bands close to yrast line. Certainly the total spectrum of gamma quanta requires also the inclusion of the statistical dipole and quadrupole gammas going from high excited states with high momenta to the yrast line states. However the contributions of these gamma quanta are not substantial as was shown in [26, 27].

Taking into account the fact that the high spin part of γ-spectrum has smooth statistical character, the intensity of γ-quanta $n_\gamma(E_\gamma)$ has to be averaged within some interval Δ of energy in the vicinity of E_γ (E_γ is the energy of γ-quantum) with some weight $\varrho_\Delta(E_\gamma)$

$$n_\gamma(E_\gamma) = \sum_{I_{\min}}^{I_{\max}} n_\gamma(I)\, \varrho_\Delta(E_\gamma - E(I)) \tag{45}$$

where sum goes over the all angular momenta of yrast-line from $I_{\min} = 2\hbar$ with step $\Delta I = 2\hbar$ up to maximal angular momentum $I_{\max}$ when nucleus exists as a bound object. Weight function has to be normalized so that

$$\int_0^\infty \varrho_\Delta(E_\gamma - E)\, \mathrm{d}E = 1\,. \tag{46}$$

Assuming weight function ϱ_Δ in the form of function of Lorentz we obtain the following expression for $n_\gamma(E_\gamma)$

$$n_\gamma(E_\gamma) = \frac{\Delta}{2\pi} \sum_{I=2}^{I_{\max}} \frac{n_\gamma(I)}{(E_\gamma - E(I))^2 + (\Delta/2)^2}\,. \tag{47}$$

In (45) and (47) $n_\gamma(I)$ stands for the number of possible quadrupole transition deexcitating the nucleus along the yrast line from the state with momentum $I_{\max}$ down

to the state with momentum I. This number $n_\gamma(I)$ is connected with the degeneracy function $g(I)$ ($\sum_I g(I) = 1$), where

$$g(I) = C\begin{cases} 2I + 1 & \text{for } I \leqq I_{\max} \\ 0 & \text{for } I > I_{\max} \end{cases} \tag{48}$$

where C is normalizing factor. Then the number $n_\gamma(I)$ is given by

$$n_\gamma(I) = C \sum_{I' \geqq I} g(I') = \frac{(I_{\max} + I + 1)(I_{\max} - I + 2)}{(I_{\max} + 1)(I_{\max} + 2)} . \tag{49}$$

The energy $E(I)$ of quadrupole transition along the yrast line from the yrast state with momentum I can be expressed as follows

$$E(I) = \frac{2I}{\Phi} \hbar \tag{50}$$

where Φ is the inertia moment of nucleus in the yrast line state with momentum I.

The calculated spectrum of gamma quanta for ^{118}Te is shown in fig. 19. The maximal angular momentum $I_{\max}$ used in eqs. (45)–(49) is $I_{\max} = 72\ \hbar$. This value was chosen in accordance with the multiplicity data [25]. The maxima in $n_\gamma(E_\gamma)$ appear just for the values of momentum I corresponding to the crossing of bands

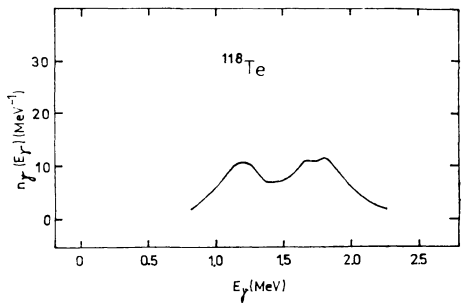

Fig. 19
The spectrum of γ-quanta $n_\gamma(E_\gamma)$ emmited by excited ^{118}Te.

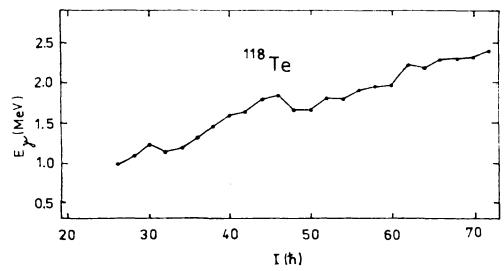

Fig. 20
The dependence of energies of γ-quanta emmited by excited ^{118}Te on angular momentum.

which form the yrast line. It is well known fact that crossing of bands leads to the irregularities in dependence of inertia moment on angular rotation frequency (see figs. 16 and 20). Because of the transition energy $E(I)$ (see (50) is proportional to $\mathscr{I}^{-1}$ the increase or reduction of inertia moment shows itself immediately as irregularity in intensity $n_\gamma(E_\gamma)$. The increase of inertia moment during the crossing of bands leads to the appearance of maximum in $n_\gamma(E_\gamma)$.

The obtained spectrum $n_\gamma(E_\gamma)$ is in qualitative agreement with the experimental data [25]. These data also provide two maxima with positions identical with calculated ones. The inclusion of the pairing correlations causes only a slight shift of the curve $n_\gamma(E_\gamma)$ in the direction of higher E_γ because the pairing correlations reduce the inertia moment.

The transition from one yrast line configuration to another one is characterized by the change in the symmetry of the average field. Therefore such a transition leads to the change of the inertia properties of nucleus and as a result of it the irregularities of the spectrum of gamma quanta deexcitating the nucleus appear. The transition from the shell regime of rotation which is characteristic for low spin region to the macroscopic liquid drop regime is accompanied by the increase of inertia moment and therefore it leads to the maximum in gamma-spectrum. From this conclusion one can see that the analysis of gamma spectrum of fast rotating nuclei resulting from (HI, xn) reaction gives the information about the shape evolution of nucleus and vice versa.

5. Emmision of alpha-particles from fast rotating nuclei

One of the most important channels of deexcitation of high excited nucleus which can occur before the gamma emission is the alpha-particle emission. Combining the microscopic approach [28] for description of alpha-decay of nonrotating nuclei with the cranking model we analyse the influence of formation factor on alpha-particle emission from high excited nucleus in high spin states [10]. It must be noted that the problem of alpha-emission from nuclear high spin states was also investigated in refs. [29, 30]. However in these papers the alpha-particle emission was treated only in the framework of the calculation of the barier penetrability in WKB approximation that means without inclusion of the effects of internal structure of nucleus.

This paper is devoted mainly to the high spin region (fast rotation). Since the pairing effects dissappear for spins $I \geqq 30\ \hbar$ (see e.g. [17]) we do not take them into account. We also restrict ourselves to the case of cold fast rotating nuclei in spite of the fact that the alpha-particle emission goes first of all from the high excited states. This is justified because we are interested in the region of excitation of nucleus after the neutron emmision which has taken away the considerable part of excitation energy. So the nucleus is in the state of cold rotation where besides the gamma emmision there is a nonzero probability of alpha-particle emission.

According to "R-matrix" theory the total width of alpha-decay from the nucleus state k is given by [28]

$$\Gamma_k = 2\pi \sum_c \left| \frac{\langle O_c^k(r) \mid \Phi_c^0(r) \rangle}{\langle O_c^k(r) \mid \Phi_c^k(r) \rangle} \right|^2 = \sum_c \Gamma_{ck} \,. \tag{51}$$

Here $O_c^k(r) \equiv r\langle \Phi_k \mid c \rangle$ is the amplitude of the factor of formation of alpha-particle in the nucleus or by the other words overlaping integral of wave function of parent nucleus $|\Phi_k\rangle$ with the internal function of α-decay channel $|c\rangle$ which consists of the internal function of α-particle and the internal function of daughter nucleus. That means the quantity $O_c^k(r)$ depends only on relative coordinates r of α-particle and daughter nucleus. The radial part $\Phi_c^{o(k)}(r)$ of the total c-channel wave function $(1/r)\,\Phi_c^{o(k)}(r)\,|c\rangle$ can be found from the following differential equation

$$\left\{ \frac{\hbar^2}{2\mu} \left[\frac{\partial^2}{\partial r^2} - \frac{L(L+1)}{r^2} \right] + V_{cc}(r) - \varepsilon_c + \sum_{c' \neq c} V_{cc'}(r) \right\} \begin{Bmatrix} \Phi_c^o(r) \\ \Phi_c^k(r) \end{Bmatrix} = \begin{Bmatrix} 0 \\ O_c^k(r) \end{Bmatrix} \tag{52}$$

where μ is the reduced mass of α-particle and daughter nucleus, $V_{cc'}$ stands for the internal matrix elements of the interaction of α-particle and daughter nucleus

$$V_{cc'}(r) = \langle c |\, V_{\alpha 0} | c' \rangle = (-1)^{I+R} (2\lambda + 1) \left[(2I+1)(2R+1) \right]^{1/2} \cdot \begin{pmatrix} L & \lambda & R' \\ 0 & 0 & 0 \end{pmatrix} \begin{Bmatrix} L & R & I \\ R' & L' & \lambda \end{Bmatrix} V_\lambda(r) \,. \tag{53}$$

Here I and R are angular momenta of maternal and daughter nucleus respectively, L is the orbital momentum of relative motion of α-particle and daughter nucleus and

$$V_\lambda(r) = \int r'^2 \varrho_\lambda(r')\, V_{\text{eff}}(|\vec{r} - \vec{r}'|)\, P_\lambda(\cos\Theta)\, \mathrm{d}r'\, \mathrm{d}\cos\Theta \tag{54}$$

where $V_{\text{eff}}(|\vec{r} - \vec{r}'|)$ is the effective interaction of α-particle and the nucleons of daughter nucleus including the Coulomb part. The symbol $\varrho_\lambda(r')$ represents the radial component of the density of nucleons of the daughter nucleus corresponding to the multipolarity λ (see e.g. [31]). The energy ε_c taken away by α-particle in channel c is given in the case of rotating nucleus by the difference of energy of parent nucleus and sum of energies of daghter nucleus and bound energy of α-particle

$$\varepsilon_c = E_\alpha(I, L) = E_I^M(\varepsilon, \gamma) - E_R^{\mathcal{D}}(\varepsilon', \gamma') - E_{\text{bound}}^\alpha \,. \tag{55}$$

In our approach the energy of material or daughter nucleus is determined from the condition of minimum of nucleus potential energy for given angular momentum I by the shell correction method of Strutinsky with the cranking Nilsson average cranking Nilsson average field [10].

The overlapping integral $O_c^k(r)$ (see (51)) can be written in the following form for the case of high angular momenta ($I \gg 1$)

$$O_c^k(r) \equiv O_{\text{LM}}^I(r) = (RRLM \,|\, II) \sqrt{\frac{2R+1}{2I+1}} \sum_k (IOLK \,|\, IK)\, \langle \omega(I) |\, A_\alpha^+(r; L, K) \,|\, \omega(R) \rangle \tag{56}$$

where $|\omega(I)\rangle$ represents the internal nucleus wave function in rotating frame (cranking model wave function), $A_\alpha^+(r; L, K)$ is the creation operator of α-particle (see [32]) depending on the overlapping integral of the internal wave function of the α-particle in the point r with the product of the wave function of four nucleons antisymmetrized with respect to variables of two protons and two neutrons [34, 35]. The overlapping integrals $O_c^k(r)$ obtained by (56) can be used in (52) for determination of $\Phi_c^{o(k)}(r)$ and the following using of (51) provides the corresponding life time of the state k of maternal nucleus with respect to α-decay through channel c

$$(T_{1/2})_{kc} = \frac{\ln 2}{\Gamma_{ck}} . \tag{57}$$

It must be noted that for zero rotation frequency we obtain the same result as in [36] for $O_c^k(r)$. In numerical calculation of partial width Γ_{ck} we did not take into account the effects of continuum. The requirement of the antisymmetrization of channel wave function in (51) was effectively involved by condition $\langle O_c^k(r) \mid \Phi_c^o(r)\rangle = 0$.

We studied the reaction $^{122}\text{Xe} \rightarrow {}^{118}\text{Te} + \alpha$ for various values of maternal as well as daughter angular momenta. We assumed that the daughter nucleus momentum was determined as $R = I - L$. The calculation of the shape evolution of the nucleus ^{122}Xe showed that the most favourable shape for medium as well as for high spins is the axially oblate form (see fig. 21). In this case the nucleus rotation has the

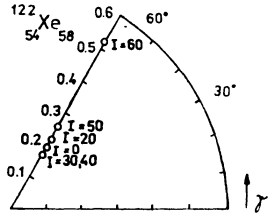

Fig. 21
The hodograph of total energy surfaces of ^{122}Xe. The points in hodographs correspond to the minimum of energy for given value of angular momentum.

"noncollective" character when the total angular momentum increases in consequence of the alignment of single nucleus along the symmetry axis. In order to avoid the numerical problems we also supposed the shape of daughter nucleus to be same as that of maternal nucleus.

The results of the calculation of the partial life time (57) in dependence on the angular momentum L of emmited α-particle are presented in fig. 22. It can be seen that for $I \leqq 36\ \hbar$ there is the minimum of $T_{1/2}$ corresponding to $L \sim 6\ \hbar$. Therefore the most of the α-particles emmited from rotating ^{122}Xe with $I \sim 36\ \hbar$ has angular momentum $L \sim 6\ \hbar$. From fig. 22 it follows that the increase of rotation momentum I leads to the reduction of half life $T_{1/2}$ and so to the increase of probability of α-

emission. Since we restricted ourselves to the case of the cold fast rotating nuclei one can conclude the following: the cold nucleus in "noncollective" fast rotation regime is the source of alpha particles.

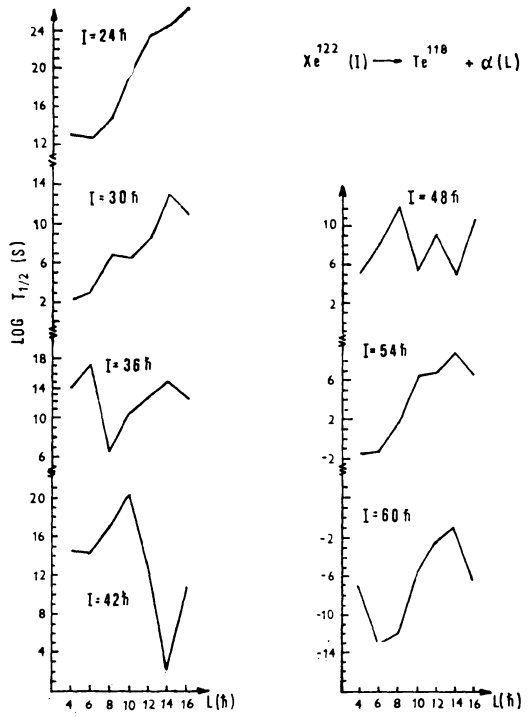

Fig. 22

The dependence of half time of α-particle on its angular momentum for different values of spins of ^{122}Xe.

The similar calculations of alpha-particle emission probability for reaction Kr → Se + α show that the taking of the formation factor into account leads to the shift of the half time $T_{1/2}$ towards the lower L in comparison with the results in [29] where the formation factor was not included. The value predicted in [29] was $L \sim 14\ \hbar$ while our results is $L \sim 8\ \hbar$. The simple estimates of the probability of nucleus deexcitation by means of the collective quadrupole gamma quanta (see expr. (3.146) in [32]) demonstrate the fact that already for $I^{II} = 34^+$ in this reaction the emission of alpha-particle is favourable channel. Indeed, the average energy of $E2$-transition in this region of angular momenta is $\Delta E_{\gamma E2} \sim 1$ MeV. Assuming that the $E2$-transition probability has the same order of value for Kr and for rare-earth deformed nuclei ($\sim 10^2$ Weisk. units) we obtain $T_{1/2}(\gamma E2) \sim 10^{-11}$ s. Our numerical minimal value of half time for α-emission is $T_{1/2}(\alpha) \sim 10^{-13}$ s.

6. Conclusions

The examples of physical effects discussed in this paper showed the importance of the shape evolution with increasing nuclear rotational frequency. The process of deexcitation of heated nucleus in high spin states is considerably influenced by the deformation of nucleus. Concretely, the way of deexcitation (particle emmision or gamma-quanta emmision) for given angular momentum is determined by the shape of nucleus. Therefore the studying of deformation or shapes of rotating nuclei is an interesting topic and determination of deformation dependence on nuclear momentum is the crucial point in understanding of the process connected with deexcitation of fast rotating and heated nucleus.

References

[1] DIAMOND R. M., STEPHENS F. S., Ann. Rev. Nucl. Part. Sci. 30 (1980) 85.
[2] GARETT J. D., HAGEMANN G. B., HEXSKIND B., Ann. Rev. Nucl. Part. Sci. 36 (1986) 419.
[3] BOHR A., MOTTELSON B. R., Proc. Int. Conf. Nuclear Structure, Tokyo 1977, J. Phys. Soc. 44 (1978) Suppl. 157–172.
[4] ANDERSSON G., LARSSON S. E., LEANDER G., et al., Nucl. Phys. A268 (1976) 205.
[5] NEERGARD K., PASHKEVICH V. V., FRAUENDORF S., Nucl. Phys. A262 (1976) 61.
[6] KVASIL J., NAZMITDINOV R. G., Acta Universitatis Carolinae-Mat. et. Phys. 29 (1988) 33.
[7] GOODMAN A. L., Hartree-Fock-Bogoliubov Theory with Application to Nuclei. in Advances in Nuclear Physics v. 11 (1979) 263.
[8] FRAUENDORF S., Nucl. Phys. A263 (1976) 150.
[9] STRUTINSKY V. M., Nucl. Phys. A122 (1968) 1.
[10] NAZMITDINOV R. G., SILISTEANU I., Sov. Nucl. Phys. 43 (1986) 58.
[11] GOODMAN A. L., Nucl. Phys. A265 (1976) 113.
[12] BANERJEE B., MANG H. J., RING P., Nucl. Phys. A215 (1973) 366.
[13] GOODMAN A. L., Finite-temperature Hartree-Fock-Bogoliubov Cranking Theory, Progr. Part. Nucl. Phys., ed. D. Wilkinson, N.Y., Pergamon Press, 1983, p. 281–310.
[14] TANABE K., SUGARAWA-TANABE K., Nucl. Phys. A406 (1983) 94.
[15] GOODMAN A. L., Nucl. Phys. A469 (1987) 205.
[16] KVASIL J., NAZMITDINOV R. G., Acta Universitatis Carolinae-Mat. et Phys. 30 (1989) 55.
[17] SZYMAŃSKI Z., Fast Nuclear Rotation, Clarendon Press, Oxford 1983.
[18] IGNATYUK A. V., MICHAILOV I. N., NAZMITDINOV R. G., MOLINA R., POMORSKI K., NERLO-POMORSKA B., Nucl. Phys. A346 (1980) 191.
[19] ROZMEY P., POMORSKI K., Nukleonika 22 (1977) 301.
[20] COHEN S., PLASIL F., SWIATECKI W. J., Ann. Phys. 82 (1974) 557.
[21] DUDEK J., MAJHOFER A., SKALSKI J., WERNER T., CWIOK S., NAZAREWICZ W., J. Phys. G5 (1979) 1359.
[22] KOLOMĚJEC V. M., MAGNER A. G., STRUTINSKI V. M., Sov. Nucl. Phys. 29 (1979) 1478.
[23] BOHR A., MOTTELSON B., Nuclear Structure, Vol. I, Benjamin N.Y., 1969.
[24] BRITT H. C., Phys. Rev. C13 (1976) 1483.
[25] DELEPLANGUE M. A., et al., Phys. Rev. Lett. 40 (1978) 629.
[26] STEPHENS F. S., Proc. Int. Conf. on Nucl. Behaviour and High Angular Momentum, Strasbourg, J. Physique 41, C10 (1980) 7.

[27] GARETT J. D., HERSKIND B., Proc. Study Weekend on Nuclei far from Stability, Daresbury, 1979.
[28] SANDULESCU A., SILISTEANU I., WUNSH R., Nucl. Phys. A305 (1978) 205.
[29] ABERG S., LEANDER G., Nucl. Phys. A232 (1979) 365.
[30] PLOrZAJCZAK M., FABER M., Phys. Rev. Lett. 43 (1979) 498.
[31] RING P., SCHUCK P., The nuclear Many-Body Problem, Springer-Verlag, N. Y. Berlin, 1980.
[32] BOHR A., MOTTELSON B., Nuclear Structure, Vol. II, Benjamin N.Y. 1974.
[33] SANDULESCU A., SILISTEANU I., Nucl. Phys. A272 (1976) 148.
[34] FURMAN V. I., HOLAN S., KADMENSKY S. G., STRATAN G., Nucl. Phys. A239 (1975) 114.
[35] MANG H. J., Ann. Rev. Nucl. Sci. 14 (1964) 1.
[36] SAWYER R. O., Atomic Nucl. Phys. Table 15 (1975) 85.
[37] POMORSKI K., NERLO-POMORSKA B., Zeit. F. Phys. A283 (1977) 383.